Organosuperelasticity

DOI: 10.1002/ange.201311014

Superelastic Organic Crystals**

Satoshi Takamizawa and Yasuhiro Miyamoto*

Abstract: *Superelastic materials (crystal-to-crystal transformation pseudo elasticity) that consist of organic components have not been observed since superelasticity was discovered in a Au-Cd alloy in 1932. Superelastic materials have been exclusively developed in metallic or inorganic covalent solids, as represented by Ti-Ni alloys. Organosuperelasticity is now revealed in a pure organic crystal of terephthalamide, which precisely produces a large motion with high repetition and high energy storage efficiency. This process is driven by a small shear stress owing to the low density of strain energy related to the low lattice energy.*

A phase transition has been observed that is maintained in a single solid state induced by heat and pressure[1,2] and by light.[3] In that transition, the solid is affected by the structural distortion that occurs during transition. In an ideal case with the conservation of one-to-one correspondence of the atoms, the solid transformation is regarded as martensitic.[4] In the special case of martensitic transformation, the material acquires superelastic characteristics (transformation pseudo elasticity), which is important from a practical viewpoint and, in fact, is expected for the wide applications to structural materials and devices. Superelastic materials are primarily developed from metallic solids such as Ti-Ni alloys, and recently from ceramics.[5,6] Superelastic material made of organic components, which satisfies the definition of superelasticity,[7] has not been obvious over eight decades since superelasticity was first discovered in a Au-Cd alloy in 1932.[8] Based on the objective state of the current research trends related to superelastic materials, it might have been considered that covalent solids, which have a high degree of interatomic interaction, only fulfill the two essential requirements when being loaded with stress on the body: 1) Conservation of the one-to-one correspondence among neighboring atoms; and 2) storage of the elastic strain, which drives the spontaneous restoring motion back to the original state. In a comparison with the covalently interatomic interaction in alloys and ceramics, the relatively weak intermolecular interaction between organic components can be unreliable for generating superelasticity in molecular solids in which, furthermore, the molecular components vary in geometry and size. In investigating an organic superelastic system, we thought that the science of superelasticity could markedly advance by material diversification and functionalization, as chemical design can be effectively applied to superelastic materials. Thus, we were looking for a pure organic superelastic body as strict and simple as possible, and found the terephthalamide crystal as the first candidate for such a superelastic material. Its superelasticity was characterized by microscopy, stress tests, and X-ray diffraction analysis.

Well-formed single crystals of terephthalamide (**1**) were obtained by recrystallization of a reagent-grade terephthalamide from hot water and used in the experiments after vacuum drying. We found that the shear stress on the crystal surface {010} of **1** bent its crystal shape in generating another crystal phase with a sharp boundary across the crystal specimen and the bending position at the phase boundary transferred upon deformation (Figure 1). The bent crystal was

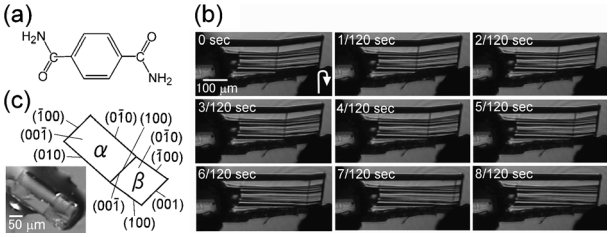

Figure 1. a) Molecular structure of **1**. b), c) Photographs of **1**: b) restoring motion after release of shear (photo interval: 1/120 s) and c) bending crystal under shear stress fixed with resin for X-ray crystal indexing.

spontaneously restored by removing the stress and the boundary transferred back by 3.33 mm s^{-1} at 298 K. (Figure 1b) The single-crystal X-ray diffraction measurement for the shear-stressed bending crystal explained the generation of the daughter crystal phase during the shear-induced transition from the mother (α phase) to the daughter (β phase; Figure 1c). The crystal packing was significantly different in the α and β crystals, while both crystal phases had the same $P\bar{1}$ crystal system.[9] The crystal structure of α had been reported previously,[10] but that of the β crystal was novel.

In the α crystal phase, terephthalamide molecules gathered to form a polymeric sheet bound by the N−H···O=C hydrogen bond network through end-to-end double hydrogen bonds (N···O distance: 2.932(4) Å) along the long axis of terephthalamide and side-to-side double N−H···O=C hydrogen bonds (N···O distance: 2.912(3) Å; Figure 2a). In the change from the α to β crystal by applying shear stress, the uniform -A-A-A-A- sheet arrangement transformed into an alternative -A′-B-A′-B- arrangement. The change in the molecular arrangement from the α into the β phase achieved a denser packing state (density: 1.470 Mg m^{-3} in α; 1.484 Mg m^{-3} in β). In the β phase, the N−H···O=C hydrogen

[*] Prof. Dr. S. Takamizawa, Y. Miyamoto
Graduate School of Nanobioscience, Yokohama City University
Seto 22-2, Kanazawa-ku, Yokohama 236-0027 (Japan)
E-mail: staka@yokohama-cu.ac.jp

[**] This work was partially supported by a Grant-in-aid for Fundamental Scientific Research (B) (Grant No. 23350028).

Supporting information for this article is available on the WWW under http://dx.doi.org/10.1002/anie.201311014.

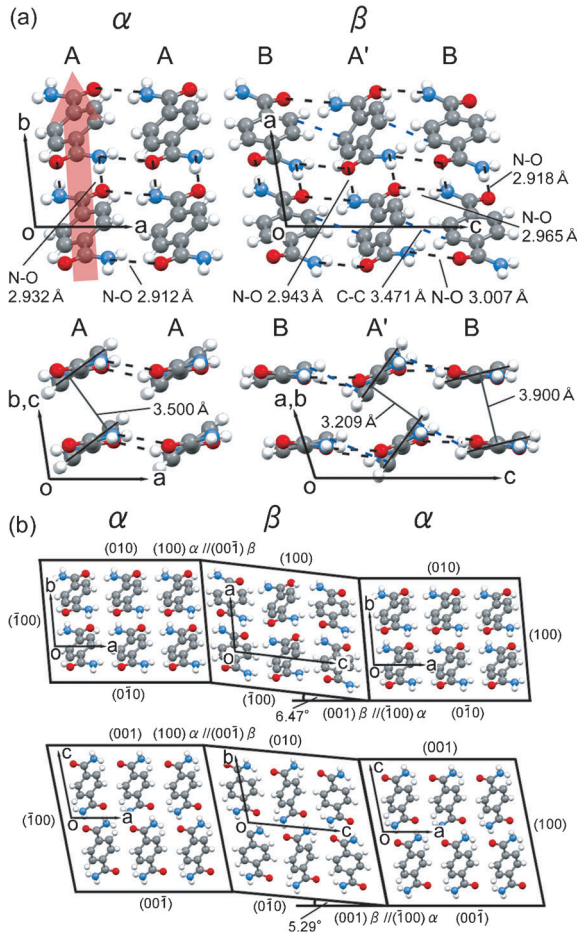

Figure 2. Elucidated phase connection under a shear-induced transition state: a) crystal packing views; b) $[00\bar{1}]_\alpha$ and $[010]_\alpha$ projection views. C Gray, H white, N blue, O red. The red arrow in (a) indicates the end-to-end coordinate. The dotted line in (a) indicates the intermolecular interaction for the NH···O=C hydrogen bond (black) and the C-H(phenyl)···C(phenyl) CH–π interaction (blue). The angles in (b) are calculated by a crossed axes angle of the normal vector of each crystal plane facing the boundary.

bond network was maintained[11] while the manner of off-set stacking of phenyl rings remarkably changed from α (surface separation: 3.500 Å) to β (surface separation: 3.209 Å in the column A′ and 3.900 Å in the column B). The shorter stacking separation in the columns A′ indicated the molecular network became rather three-dimensional in the β phase (Figure 2a). The martensitic boundary parallel with the $(100)_\alpha$ plane is almost orthogonal to the easy cleavage plane $(011)_\alpha$, which lies in the layer of the hydrogen bonding sheets. The disparity between the boundary plane and the cleavage plane can make the transformation stable against distortion around the interface. X-ray diffraction data collected in the bending form indicated how each crystal fits at the interface under the α/β coexistent state. In the $(100)_\alpha//(00\bar{1})_\beta$ interface, the ratio of the facing area is 0.989 for S_α/S_β, which raises the Bain distortion. At the interface, the α and β crystal faces should respectively feel a force of face extension and contraction. In detail, the certain difference in the length of *c* axis(α) and *b* axis(β) ($c(\alpha)$ (7.1853 Å)//$b(\beta)$ (7.268 Å) indicates the mainly unidirectional distortion along the *c* axis in the α face and along the *b* axis in the β face, respectively.

The deduced connection view at the interface (Figure 2b) clearly revealed the martensitic mechanism assisted by the change of molecular packing way. The directions in [010] and $[00\bar{1}]$ in α crystal can be effective axes for shear-induced transformation. With a microscope, the bending angles were observed to be in the range of 5–8° and 3–5° judged from the projection directions of [001] and [010], respectively, which agree with the expected angles from the X-ray data in 6.47° and 5.29°, respectively (Figure 2b). The proportion in the displacements of the pushing position on the $(010)_\alpha$ surface and the moving (far) side of the β/α interface was 1:6.7, which agrees approximately with the expected value of 1:5.4 using the X-ray crystal data. The agreement to the structural description demonstrates the harmonious support of the macro- and microscopic structural changes in **1**.

The relationship between shear stress and strain was investigated by loading on the portion of crystal surface $\{010\}_\alpha$, which should be nearly parallel to the shear-transition easy axis (see Figure 2b). After one end of a single-crystal was fixed, a metal blade (25 μm wide) was pushed across the $(010)_\alpha$ surface of the crystal specimen at a constant speed of 500 μm min^{-1}. The transformation of **1** was captured precisely (Figure 3). Stress was detected at (a) after the blade reached the crystal and began increasing the phase boundary with a linear increase in loading force (photographs 1–5 in Figure 3a). Then, the stress became constant at (b) where the thin band of the β phase was generated from the contact part of the blade. The plateau continued during the growth and propagation of the β phase by the continuous proceeding of the α–β transition (c,d). At the switching point for the unloading process (pulling the blade back) (e), a slight decrease in stress was observed and it continued in maintaining a plateau during the phase change of the β phase into the α phase (f,g) until the β domain narrowed to the boundary line (h). At that point, the stress was linearly decreased down to zero along the vanishing line boundary (6–10) until the blade was removed from the crystal surface (i). The observed shear–stress curve clearly demonstrated the superelasticity in **1**. The superelastic transformation of **1** was reproduced in 100 cycles of measurements without any elastic reduction or material cure (see the insets in Figure 3b and c). The cycling tests on single crystals with different dimensions showed that the strength of stress generated under the bent shape is linear with the area of the boundary and is not related to the contact area of pushing (Supporting Information, Figure S7). This means that the elastic index for a shear of **1** should be normalized by the absolute force divided by the area of the α–β boundary, which corresponds with the definition of the shear stress that is the force divided by the cross-section area of the specimen: 4.96×10^5 N m^{-2} (0.496 MPa at b) for transformation (σ_M) and 4.59×10^5 N m^{-2} (0.459 MPa at h) for the reverse transformation. A shear stress of **1** is one thousand times smaller than 558 MPa, which is the known value for the typical Ti-Ni alloy (see Figure 4).[12] The energy storage density (E) and energy storage efficiency (η) of **1** were estimated at 0.062 MJ m^{-3} and 0.925, respectively. The movable range of superelastic shear strain is wide, up to

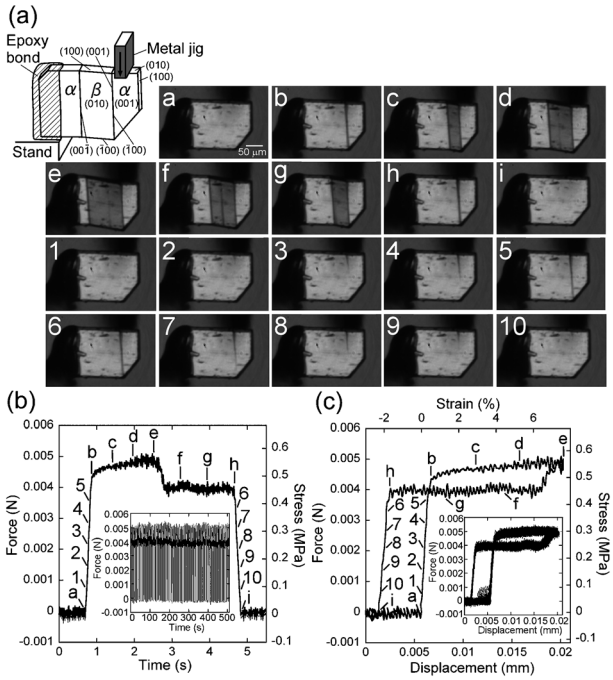

Figure 3. Results of a shear stress test for single-crystal **1** (149.52 μm thick and 58.84 μm wide) in a displacement speed of 500 μm min^{-1} at 294 K. Side-view photographs a) taken with a polarization microscope (moved 10° from the crossed Nicols angle) during the shear-strain test with the letters and numbers showing the position in the figures (b) and (c) for the time course and the displacement course, respectively. In (b) and (c), the normalized stress in the right axis denotes the shear stress that is the force divided by the cross-section area of the crystal. The inset graphs are the profiles at the 100 cycles; the first cycle is displayed as the main graph.

11.34%, which can be predicted by the geometrical arrangement of the junction of the adjacent crystal lattices with the crystal data.

Terephthalamide is a superelastic body, which was first discovered in an organic solid. Its energy storage density is 62 kJ m^{-3} (0.042 J g^{-1}, 6.96 J mol^{-1}, which is 226 times less than that of 14 MJ m^{-3} (2.15 J g^{-1}, 114.76 J mol^{-1}) for a typical Ti-Ni alloy.[12] The energy storage ability is related to the lattice energy since the ratio in the energy storage densities (6.96 J mol^{-1}(**1**):114.76 J mol^{-1}(Ti-Ni) = 1:16.5) agrees with the ratio in the bonding energy (4 × 28.87 kJ mol^{-1} (NH···O=C)[13]:4 × 458.83 kJ mol^{-1} (Ti-Ni)[14] = 1:15.9). Because of the component's bulkiness, the volumetric energy density becomes smaller by the extent of the lattice. Consequently, superelastic molecular material can produce a large transformation from a small energy input, and, vice versa, can generate a uniform level of small power with a large reverse transformation. This work demonstrated the efficiency of noncovalent interaction to produce superelasticity with accuracy, which offers more precise controllability than those of metal alloys (Figure 4). Considering currently expected applications of superelastic alloys, we believe that organic-related crystals have the potential newness to develop the new elastic materials by the introduction of chemical design from a structural and functional viewpoint.

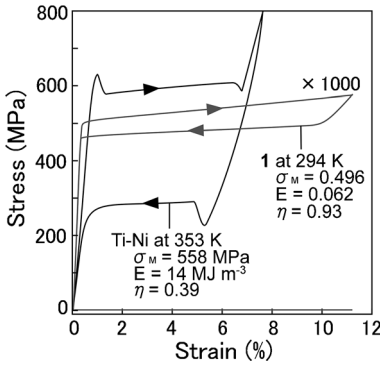

Figure 4. Superelastic characteristics of **1** in comparison with a Ti-Ni alloy.[12]

Received: December 19, 2013
Revised: March 10, 2014
Published online: May 5, 2014

Keywords: amides · crystal engineering · mechanical properties · phase transitions · terephthalamide

[1] H. G. Brittain in *Polymorphism in pharamaceutical solids*, 2nd ed., Informa Healthcare, New York, **2009**.
[2] A. D. Bond, *Curr. Opin. Solid State Mater. Sci.* **2009**, *13*, 91–97.
[3] S. Kobatake, S. Takami, H. Muto, T. Ishikawa, M. Irie, *Nature* **2007**, *446*, 778–781.
[4] K. Bhattacharya in *Microstructure of martensite: Why it forms and how it gives rise to the shape-memory effect*, Oxford University Press, Croydon, **2003**.
[5] Z. G. Wei, R. Sandstrom, S. Miyazaki, *J. Mater. Sci.* **1998**, *33*, 3743–3762.
[6] K. Otsuka, C. M. Wayman in *Shape memory materials*, Cambridge University Press, Cambridge, **1998**.
[7] C. M. Wayman, J. D. Harrison, *JOM* **1989**, *41*, 26–28.
[8] A. Ölander, *J. Am. Chem. Soc.* **1932**, *54*, 3819–3833.
[9] Crystal data for the α phase at 297 K in 0.1 MPa air: Triclinic, $P\bar{1}$, $a = 5.0238(12)$, $b = 5.3870(13)$, $c = 7.1853(18)$ Å, $\alpha = 103.413(5)$, $\beta = 100.286(5)$, $\gamma = 92.374(6)°$, $V = 185.41(8)$ Å^3, $Z = 1$, $d_{calcd} = 1.470$ Mg m^{-3}, $R_1 = 0.0646$ (0.1221), $wR_2 = 0.1495$ (0.1787) for 530 reflections with $I > 2\sigma(I)$) (for 918 reflections (1396 total measured)), goodness-of-fit on $F^2 = 0.995$, largest diff. peak (hole) = 0.339 (−0.204) e Å^{-3}. The α phase in the α–β bending form at 298 K: Triclinic $P\bar{1}$, $a = 5.030(3)$, $b = 5.395(3)$, $c = 7.202(2)$ Å, $\alpha = 103.413(14)$, $\beta = 100.269(13)$, $\gamma = 92.382(13)°$, $V = 186.35(19)$ Å^3, $Z = 1$, $d_{calcd} = 1.463$ Mg m^{-3}, $R_1 = 0.1016$ (0.1099), $wR_2 = 0.2870$ (0.2969) for 457 reflections with $I > 2\sigma(I)$) (for 529 reflections (911 total measured)), goodness-of-fit on $F^2 = 1.245$, largest diff. peak (hole) = 0.567(−0.397) e Å^{-3}. The β phase in the α–β bending form at 298 K: Triclinic $P\bar{1}$, $a = 5.3663(17)$, $b = 7.268(2)$, $c = 10.160(3)$ Å, $\alpha = 104.149(7)$, $\beta = 97.699(7)$, $\gamma = 102.672(7)°$, $V = 367.4(2)$ Å^3, $Z = 2$, $d_{calcd} = 1.484$ Mg m^{-3}, $R_1 = 0.0868$ (0.1045), $wR_2 = 0.2292$ (0.2468) for 1001 reflections with $I > 2\sigma(I)$) (for 1295 reflections (2118 total measured)), goodness-of-fit on $F^2 = 1.125$, largest diff. peak (hole) = 0.550 (−0.412) e Å^{-3}. CCDC 977998, 977999, and 978000 contain the supplementary crystallographic data for this paper. These data can be obtained free of charge from The Cambridge Crystallographic Data Centre via www.ccdc.cam.ac.uk/data_request/cif.
[10] R. E. Cobbledick, R. W. H. Small, *Acta Crystallogr. Sect. B* **1972**, *28*, 2893–2896.

[11] The strength in the NH···O=C interaction was fluctuated in the β crystal phase due to the -A′-B-A′-B- arrangement. There are the end-to-end NH···O=C (2.943(5) Å (N(A′)···O(A′)) and 2.918(5) Å (N(B)···O(B)) and the side-to-side NH···O=C (3.007(4) Å (N(A′)···O(B)) and 2.965(4) Å (N(B)···O(A′)) with the aid of the CH–π interaction in the side-to-side direction (C_{phenyl}(B)···C_{phenyl}(A′): 3.471(6) Å), which assists the stability in the sheet structure (see the right picture in Figure 2a).
[12] E. Pieczyska, S. Gadaj, W. K. Nowacki, K. Hoshio, Y. Makino, H. Tobushi, *Sci. Technol. Adv. Mater.* **2005**, *6*, 889–894.
[13] D. Tzeli, L. D. Petsalakis, G. Theodorakopoulos, D. Ajami, J. Rebek, Jr., *Int. J. Quantum. Chem.* **2013**, *113*, 734–739.
[14] Z. Lei, L. Shichun, *Cailiao Daobao* **2001**, *25*, 126–130.

